Research Article Vol. 27, No. 25 / 9 December 2019 / Optics Express 36731

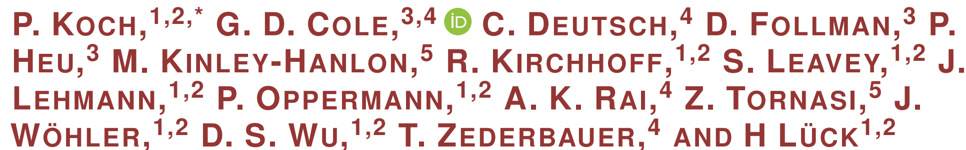

Thickness uniformity measurements and damage threshold tests of large-area GaAs/AlGaAs crystalline coatings for precision interferometry

P. KOCH,[1,2,*] G. D. COLE,[3,4] C. DEUTSCH,[4] D. FOLLMAN,[3] P. HEU,[3] M. KINLEY-HANLON,[5] R. KIRCHHOFF,[1,2] S. LEAVEY,[1,2] J. LEHMANN,[1,2] P. OPPERMANN,[1,2] A. K. RAI,[4] Z. TORNASI,[5] J. WÖHLER,[1,2] D. S. WU,[1,2] T. ZEDERBAUER,[4] AND H LÜCK[1,2]

[1] *Albert-Einstein-Institut/ Max-Planck-Institut for Gravitaional Physics, D-30167 Hannover, Germany*
[2] *Leibniz Universität Hannover, D-30167 Hannover, Germany*
[3] *Crystalline Mirror Solutions LLC, Santa Barbara, CA 93101, USA*
[4] *Crystalline Mirror Solutions GmbH, A-1010 Vienna, Austria*
[5] *SUPA, School of Physics and Astronomy, University of Glasgow, Glasgow G12 8QQ, UK*
[*] *philip.koch@aei.mpg.de*

Abstract: Precision interferometry is the leading method for extremely sensitive measurements in gravitational wave astronomy. Thermal noise of dielectric coatings poses a limitation to the sensitivity of these interferometers. To decrease coating thermal noise, new crystalline GaAs/AlGaAs multilayer mirrors have been developed. To date, the surface figure and thickness uniformity of these alternative low-loss coatings has not been investigated. Surface figure errors, for example, cause small angle scattering and thereby limit the sensitivity of an interferometer. Here we measure the surface figure of highly reflective, substrate-transferred, crystalline GaAs/AlGaAs coatings with a custom scanning reflectance system. We exploit the fact that the reflectivity varies with the thickness of the coating. To increase penetration into the coating, we used a 1550 nm laser on a highly reflective coating designed for a center wavelength of 1064 nm. The RMS thickness variation of a two inch optic was measured to be 0.41 ± 0.05 nm. This result is within 10% of the thickness uniformity, of 0.37 nm RMS, achieved with ion-beam sputtered coatings for the aLIGO detector. We additionally measured a lower limit of the laser induced damage threshold of 64 MW/cm^2 for GaAs/AlGaAs coatings at a wavelength of 1064 nm.

© 2019 Optical Society of America under the terms of the OSA Open Access Publishing Agreement

1. Introduction

Current generation gravitational wave detectors are sensitive Michelson interferometers designed to be limited by thermal and quantum processes [1]. These systems are capable of measuring length changes with an amplitude spectral density below 10^{-18} m/Hz$^{1/2}$ in a frequency band ranging from 20 Hz to 7 kHz. Coating thermal noise and quantum noise limit the sensitivity above 20 Hz [2].

Newly developed substrate-transferred crystalline coatings offer promising characteristics for such precision interferometers, including reduced thermal noise [3], sub-ppm absorption [4], and ppm-level scattering [5]. In this process, alternating layers of gallium arsenide (GaAs) and aluminum gallium arsenide ($Al_{0.92}Ga_{0.08}As$) are grown on a GaAs wafer in a molecular beam epitaxy (MBE) chamber. These single-crystal films are then removed from their initial growth wafer and transferred to a fused silica substrate using a direct bonding process. This substrate-transfer process have been covered in detail in previous publications including [3] and [4]. The low mechanical loss of crystalline GaAs/AlGaAs multilayers leads to a reduced

#375550 https://doi.org/10.1364/OE.27.036731
Journal © 2019 Received 16 Aug 2019; revised 2 Oct 2019; accepted 15 Oct 2019; published 4 Dec 2019

coating thermal noise. Their optical properties and the manufacturing process result in sub-ppm absorption and ppm level scattering.

However, it remains to be shown that the surface figure of GaAs/AlGaAs coatings fulfills the requirements of km-scale gravitational wave detectors. While point defects and microroughness determine wide angle scattering, the mirror surface figure is mostly responsible for low angle scattering. Thereby an imperfectly spherical mirror will scatter light into higher order modes. To avoid that this reduces the gravitational wave detectors sensitivity, a surface flatness of below 0.3 nm RMS was specified for Advanced LIGO (aLIGO) and Advanced Virgo (aVirgo) [6].

Here we show that the thickness uniformity of current GaAs/AlGaAs coatings comes very close to the requirements of gravitational wave detectors with a level comparable to ion-beam sputtered (IBS) coatings. Ignoring potential imperfections from the substrate-transfer process, the thickness uniformity is the contribution of the coating to the surface figure of a mirror. We measured a thickness uniformity of 0.41 ± 0.05 nm RMS. This is within 10% of the achieved thickness uniformity of 0.37 nm RMS for IBS coatings in the aVirgo detector [7]. In addition to this result we present a method for measuring the thickness uniformity of dielectric coatings to a sub 0.1 nm level.

Knowing the coating structure, a reflectivity map of a dielectric coating can be converted into a thickness uniformity map. The reflectivity of such a coating is directly dependent on the thickness of each individual layer. Assuming that each pair of alternating layers is grown equally, the total thickness can be calculated from the reflectivity. Here the probe wavelength differs from the design wavelength to penetrate all layers of the coating. An angle of incidence was chosen which maximizes the reflectivity dependence on the total thickness of the coating.

We further present two possible methods to suppress the influence of reflected light from a mirror's non-coated rear surface (see section 3.). The first is index-matched bonding to a ground substrate which scatters the otherwise reflected light. For the second method, two measurements with different interference conditions of the rear reflection are combined.

In addition we measured a lower limit of the laser induced damage threshold (LIDT) for a GaAs/AlGaAs coating (see section 7.). High finesse cavities, created with highly reflective mirrors, have the possibility of damaging the mirror coatings if the light field strength exceeds the LIDT. The mirror used for this experiment was nominally identical to that used for the thickness uniformity measurements. We focused an 85 W continuous wave laser with a wavelength of 1064 nm to a spot size of 9.2 μm radius resulting in a peak power density of 64 MW/cm^2. This sets a lower limit for the LIDT of the mirror sample as no damage was observed. The measured LIDT value is well above the requirements of aLIGO with 17 kW/cm^2 (based on [8]).

2. Thickness uniformity measurements of dielectric coatings

In this section we describe a method to measure the thickness uniformity of highly reflective, dielectric coatings. The method is discussed in the context of quarter-wave coating stacks assuming that all layers contribute equally to the total coating thickness. Under this assumption the method can also be applied to other coating structures. The reflectivity simulations for dielectric coatings at arbitrary angles of incidence in this section used the `multidiel` code [9] for MATLAB. This code is based on the electromagnetic wave functions as described in [10].

A highly reflective coating can be designed for a specific wavelength (λ_0) by combining alternating quarter wave layers of two materials with different refractive indices. Each refractive index boundary reflects a small portion of the incident light. The optical path length of a layer is defined as its geometrical thickness (t) multiplied by its refractive index (n). A constructive interference between reflections of different boundaries arises for an optical path length of $\lambda_0/4$ (Eq. (1) [11]). Thereby the light acquires 180 deg phase on reflection. A reflection from a low (L)-to-high (H) refractive index boundary leads to an additional phase shift of 180 deg. For each additional bilayer a fraction of the light is reflected and constructively interferes with the

Optics EXPRESS

previously reflected light.

$$n_H \cdot t_H = n_L \cdot t_L = \frac{\lambda_0}{4} \, [11] \quad (1)$$

Changing the incident wavelength or the total thickness similarly affects the reflectivity of an interference coating; if either changes, the optical path length between two layers will not provide full constructive interference, reducing the reflectivity of the coating. In Fig. 1, the reflectivity is plotted as a function of the incident wavelength for two different coating thicknesses.

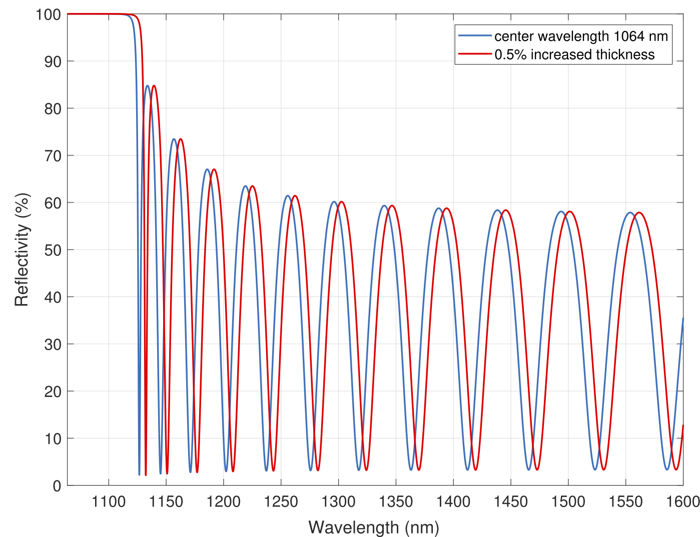

Fig. 1. Simulated reflectivity spectrum of two high reflectivity GaAs/AlGaAs coatings with 35.5 bilayers at normal incidence. One designed for 1064 nm wavelength (blue) and the other differing by an increased thickness of each layer by 0.5% (red).

A varying reflectivity of the coating can be converted into a thickness variation for a fixed wavelength and angle of incidence. The angle of incidence and the refractive indices result in a reflection coefficient according to the Fresnel equations. The reflectivity of the coating is, therefore, only affected by the total coating thickness and the incident wavelength assuming a constant error factor for all layers (see Eq. (1) and Fig. 1). A conversion function can be determined by plotting the reflectivity against the total thickness variation at a given wavelength.

The dependence of the reflectivity on the total layer thickness can be maximized by changing the incident wavelength. At λ_0, the reflectivity is close to one, as designed. Thus, the first few bilayers reflect a large majority of the incident optical field. This reduces the contribution of the underlying bilayers to the overall reflectivity. Figure 1 further shows that the reflectivity change between the two coating thicknesses at λ_0 is close to zero. Moving off of the high-reflectivity stopband enables greater penetration of light into the coating stack and increases the reflectivity dependence on the coating thickness. Figure 1 also shows that a steeper slope of the reflectivity spectrum results in a larger change of the reflectivity between the two coating thicknesses. In the example of Fig. 1 a wavelength around 1550 nm could be used.

The angle of incidence can additionally be used to fine-tune the slope of the reflectivity spectrum at a chosen wavelength. The change of the angle of incidence will change the reflectivity in two different ways. First as described by the Fresnel equation and second through the increased propagation phase shift of the light through each coating layer. The second effect is equivalent to a homogeneous change of the total layer thickness. Hence, the reflectivity spectrum (Fig. 1) can be shifted to maximize the slope for a particular wavelength. This shifting though is limited

by the impracticality of measuring at high angles of incidence which partly depends on the measurement set-up. Using a wavelength of 1064 nm on the mirror simulated in Fig. 1 would require an impractical angle of incidence of above 60 degrees to maximize the slope of the reflectivity spectrum. However, for a wave length of 1550 nm an angle of incidence of 20 deg can be used to maximize the reflectivity dependence on the coating thickness.

3. Compensating a rear surface reflection

As an uncoated rear surface can influence the measurement, this section presents two different methods to reduce the power of light reflected from the rear surface of the substrate.

The reflection from the rear surface of a substrate influences the total reflectivity of a mirror. The boundary between fused silica and air reflects about 4% of the incident power in the near infrared spectral region, which is a non-negligible portion of the otherwise transmitted light. This reflection interferes with the light reflected from the coating depending on its phase accumulated as it propagates through the substrate.

The thickness uniformity measurement relies on the fact that the reflectivity is only influenced by the coating thickness. A non-uniform substrate thickness leads to a varying and position dependent interference condition. Thus, the total reflectivity varies with the thickness of the substrate. With a parasitic reflection from the rear surface of the sample it is not possible to separate variations in the coating uniformity from changes of the substrate thickness. Here we discuss two ways in which influence of the rear surface reflection can be eliminated.

3.1. Averaging of phase shifted measurements

A change of the angle of incidence influences the interference condition of the light reflected from the rear surface more than of the light reflected from the coating. The thickness of a high-reflectivity coating (t_c) is small compared to the thickness of its substrate (t_s). Thus, a change of the angle of incidence changes the path length through the substrate by the ratio t_s/t_c than the path length through the coating.

Two reflectivity measurements at slightly different angles can be combined to average out the backside reflection from the substrate. A change of the angle of incidence ($\Delta\alpha$) modifies the path lengths (l_1, l_2) through the substrate between two measurements. The effect of the rear reflections for these two measurements is opposite if their phase differs by 180 deg. Thus, $\Delta\alpha$ has to change the optical path length through the substrate by $\lambda/4$. The angle of incidence α_2 for the second measurement can be calculated as shown in Eq. (3) derived by Eq. (2), trigonometric functions and Snell's law.

$$l_2 = \frac{\lambda}{4 \cdot n} + l_1 \tag{2}$$

$$\alpha_2 = \arcsin \frac{n}{n_0} \cdot \sqrt{1 - \left(\frac{t_s}{\lambda \cdot (4 \cdot n)^{-1} + t_s \cdot (\sqrt{1 - (n_0 \cdot n^{-1} \sin \alpha_1)^2})^{-1}} \right)^2}, \tag{3}$$

where t_s is the thickness and n the refractive index of the substrate and n_0 is the refractive index of the surrounding medium. λ is the laser wavelength and α_1 is the angle of incidence of the first measurement. The corresponding path length change through the coating is well below $\lambda/1000$ assuming that the substrate is about 1000 time thicker than the coating.

3.2. Scattering and index-matched bonding

Index-matched bonding to a non-reflecting substrate can be used to eliminate the influence the reflection from the rear surface completely. The reflectivity of a boundary depends on the refractive index difference of the consecutive materials as described by the Fresnel equations. Hence, a boundary will not reflect light when two substrates of the same material are bonded with

Optics EXPRESS

a fluid matching their refractive index. We used a substrate with ground surfaces creating diffuse reflection to scatter incident light. This redistributes the reflected power of the rear surface over a larger solid angle reducing the power which can interfere with the light reflected from the coating. Figure 2 shows such an index-matched bond between two fused silica substrates using glycerol, with refractive indices shown for incident light at a wavelength of 1550 nm.

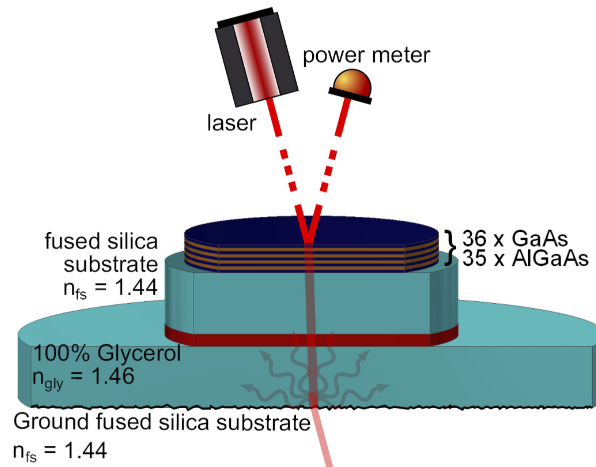

Fig. 2. The GaAs/AlGaAs coating consisting of 35.5 bilayers bonded to a fused silica substrate. Glycerol is used as an index-matched bonding fluid to bond the mirror to a ground fused silica substrate. The transmitted laser light is scattered at the ground surface of the second substrate instead of being directly reflected towards the power meter. The refractive index difference between fused silica (fs) [12] and glycerol (gly) [13] at a wavelength of 1550 nm is Δn = 0.02.

4. Experimental set-up

This section describes the measurement set-up as well as the individual steps to measure the thickness uniformity of a dielectric coating.

A scanning device and components for a reflectivity measurement were needed for the thickness uniformity measurement of an interference coating. The mirror to be measured is placed on a translation stage. The translation stage allows movements in horizontal and vertical directions as well as rotation around the vertical axis. A $\lambda/2$-plate in combination with a polarizing beam splitter polarizes the laser light linearly into a desired orientation (here p-polarization). Lenses first collimate and then focus the laser onto the sample to a spot size of 1 mm. A power meter in the pick-off beam from the polarization beam splitter with a known splitting ratio measures the incident light power. Power meters in either the reflected or transmitted path measure the reflected or transmitted power. The ratio of incident to reflected or transmitted light power is the reflectivity or transmission of the mirror respectively. This set-up can be seen in Fig. 3. At each spot position on the mirror, the reference power and the reflected power were averaged over one second and the reflectivity calculated. The entire surface of the coating was scanned by moving the mirror using the two-dimensional translation stage. The reflectivity values were converted into thickness uniformity values by comparing to a modeled coating structure, as described in section 2. A thickness uniformity map can be generated from these values.

We used two linear stages with a minimum step size of 1 μm at a repeatability accuracy of 20 μm as translation stage. The employed rotation unit has a minimum step size of 0.04 deg and a repeatability accuracy of 0.015 deg. For the power meters, we used Thorlabs S132C photodiode

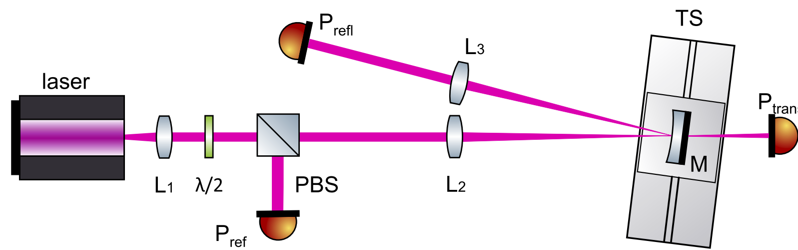

Fig. 3. A laser is collimated by a lens (L_1), then polarized by a polarization plate ($\lambda/2$) and a polarizing beam splitter (PBS). It is then focused by L_2 (f = 500 mm) onto the sample M mounted on a translation stage (TS). A reference beam is picked of by the PBS and measured by a power meter (P_{ref}). L_3 (f = 500 mm) collimates the reflected beam which is measured by P_{refl}. The transmitted power can be measured with P_{trans}.

power sensors. They provide a resolution of 1 nW at a measurement uncertainty of 5%. We used a 10 mW DFB laser diode, which was temperature stabilized using a Peltier element. The power noise of the laser diode in combination with technical noise of the power meters was measured to be by far the dominating noise source in our set-up resulting in an uncertainty of 0.03%.

5. Thickness uniformity results

In this section we present the results of a thickness uniformity measurement (Fig. 4) using the method described in section 2.

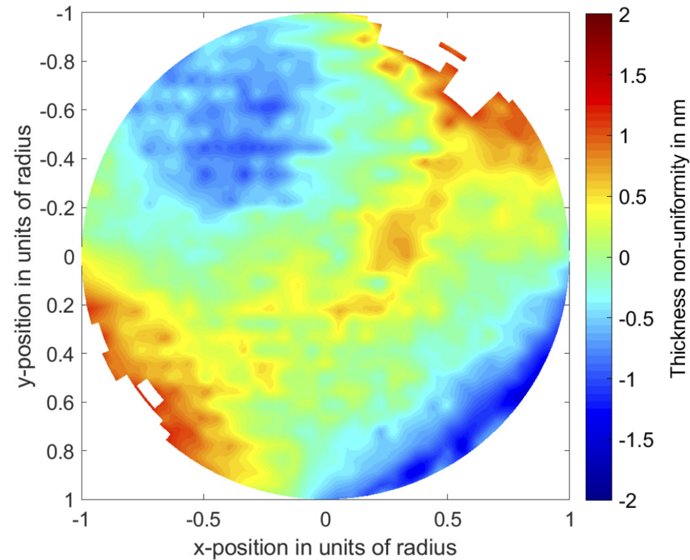

Fig. 4. Thickness uniformity of the two inch GaAs/AlGaAs sample. Scan resolution of 10 measurements per cm. The Zernike polynomials of zeroth, first, and second order were subtracted. The outermost 2 mm as well as a defect near the rim were ignored for the RMS calculation.

Here, the thickness uniformity of a highly reflective crystalline GaAs/AlGaAs coating was measured. This coating consisted of 35.5 bilayers with a nominal transmission of 10 ppm at a center wavelength of 1064 nm. Each bilayer consists of one layer of GaAs and one layer of $Al_{0.92}Ga_{0.08}As$. The refractive indices $n_{GaAs} = 3.480$ and $n_{AlGaAs} = 2.977$ were measured

by the manufacturer. They define the individual layer thicknesses to t_{GaAs} = 76.43 nm and t_{AlGaAs} = 89.35 nm. The 45 mm diameter sample was cut from a 6 inch wafer located at the center position of the MBE chamber during the coating run (see Fig. 5). No coating was applied to the rear surface of the one millimeter thick fused silica substrate.

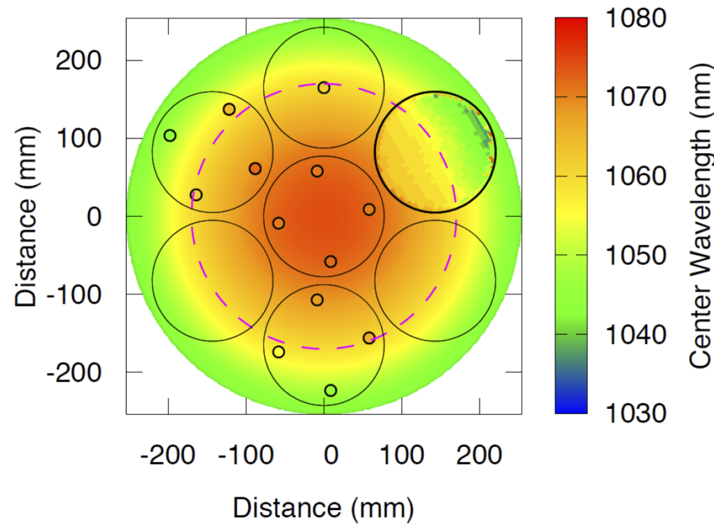

Fig. 5. Layout of the seven 15 cm diameter GaAs wafers within the Veeco Gen2000 MBE chamber. The thickness uniformity across the platen is determined by measuring the thickness of 13 1 cm diameter witness pieces (indicated by the small circles in the central and orbital wafers). Additionally we have performed a position-dependent reflectivity measurement via spectrophotomery on one of the orbital wafers (upper right position).

An accuracy of the thickness uniformity of 0.05 nm was achieved in the measurement. A local maximum of the reflectivity dependence on the total coating thickness was found for a wavelength of 1550 nm and a fixed angle of incidence of 20 deg. The resulting conversion factor from reflectivity to thickness uniformity was 1.41 nm/%. The accuracy was limited by technical noise of the laser and the power meters. Here, a standard deviation of 0.03% reflectivity was measured at a constant mirror position. The reflections from the non-coated rear surface have been suppressed by a factor of 70 as described in section 3.

A thickness uniformity of 0.41 ± 0.05 nm was measured including a correction of Zernike polynomials (Z_n^m) of zeroth, first, and second order. An adjustment of the mirror position can compensate piston, tilt and spherical errors. Thus, the corresponding Zernike polynomials have been removed before the RMS calculation. Z_0^0 describes the piston error and was corrected by 13.3 nm. Z_1^{-1} and Z_1^1 describe the tilt error along the vertical and horizontal axis and were corrected by 57 nrad and 70 nrad. Z_0^2 describes the spherical error and was corrected by 0.024 km^{-1}. The outermost 2 mm of the coating and a defect near the rim, which formed during the bonding process have been ignored. The thickness uniformity map can be seen in Fig. 4.

As the sample represents only a fraction of the coating produced during the epitaxial growth run, additional measurements of the overall thickness distribution within the MBE chamber were made. Seven 6 inch diameter wafers were grown during a single growth run. High resolution X-ray diffraction [14] was used on different spots on four of these wafers to determine the thickness of the individual layers and the aluminum mole fraction of the AlGaAs. The location of these spots can be seen in Fig. 5 as small circles on the individual wafers. Furthermore, Fig. 5 includes a spectrophotometer scan performed on one of the orbital wafers. The results were used

Optics EXPRESS

to calculate the local center wavelength of the coating. Figure 6 shows the center wavelength plotted against the distance of each point from the center of the MBE chamber.

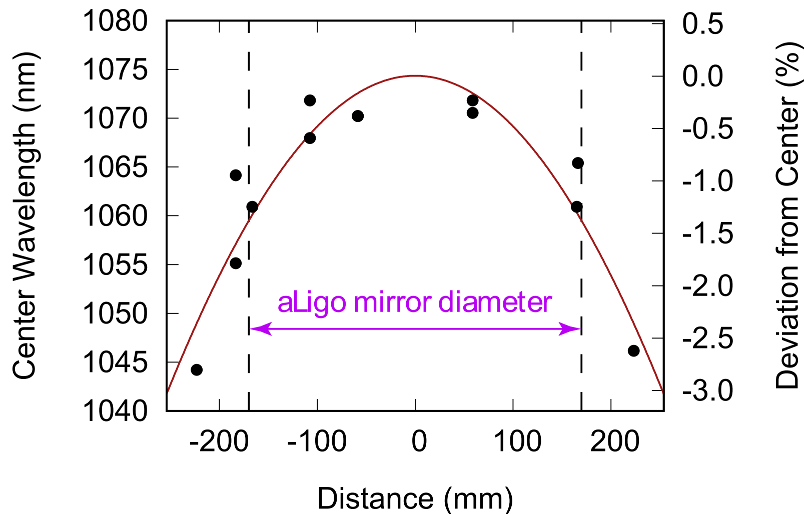

Fig. 6. Extracted thickness uniformity for the epitaxial coating across the growth platen fitted to the X-ray diffraction measurements on the small witness pieces.

6. Discussion

This section compares the measured thickness uniformity of a crystalline GaAs/AlGaAs coating with IBS coatings and the current requirements of gravitational wave detectors.

The measured thickness uniformity of the GaAs/AlGaAs coating comes very close to the requirements of km-scale gravitational wave detectors. The required surface flatness of the mirrors used by aLIGO and aVirgo was set to <0.3 nm RMS on the inner 16 cm diameter [6]. The incoherent sum of the surface error of the substrate and the thickness uniformity of the coating determines the surface error of the mirror. The surface error of the substrates of the test mass mirrors installed at the aLIGO detectors ranges from 0.08-0.23 nm RMS in the central area within a diameter of 16 cm. These values had the piston, tilt and astigmatism removed from the measurement [8]. Thus, the thickness uniformity measured for the 4 cm diameter GaAs/AlGaAs coating comes very close to these requirements with an RMS of 0.41 nm.

In terms of prospects for large-area coatings, the thickness variation over the central 30 cm diameter of the platen remains below 1% as can be seen in Fig. 6. However, approaching the full 34 cm diameter of advanced detector optics, the coating center wavelength (proportional to the thickness) shifts by as much as 1.5%. With optimization of the molecular beam profile, we are confident that this can be significantly reduced to maintain a total thickness variation <1% over this diameter. Recent investigations of the MBE growth of high-uniformity vertical-cavity surface-emitting lasers (VCSELs) have shown the potential for thickness variations at the 0.3% level over the same area [15], making crystalline coatings amenable to next-generation gravitational wave detectors.

The thickness uniformity found for the GaAs/AlGaAs coatings is comparable to the IBS coatings used in aLIGO and aVirgo. In contrast to GaAs/AlGaAs coatings, IBS coatings are directly deposited onto a substrate [16]. For aVirgo, a coating thickness uniformity of 0.37 nm RMS was achieved on a substrate polished to a surface error of 0.19 nm RMS. The substrates of the aLIGO optics were polished to a surface error of 0.18 nm RMS. The surface error of the mirror was then measured to 0.69 nm RMS after deposition of the coating [8].

The accuracy of the thickness uniformity measurements of dielectric coatings using the method explained here can be further improved by reducing technical noise. Broadband power meters can be replaced with low noise photo diodes to increase the sensor sensitivity. Furthermore, an amplitude stabilization servo can be installed to reduce power fluctuations which couple directly into the measured thickness uniformity. A stronger dependence of the reflected light on the total coating thickness can be achieved by using a laser wavelength of 1150 nm and some fine tuning using the angle of incidence as described in section 2.

7. Damage threshold tests

In this section we aimed to measure a laser induced damage threshold (LIDT) of the GaAs/AlGaAs coating itself trying to exclude voids, defects and particles.

The optical field strength which leads to damage or destruction of a coating is defined as the LIDT. There are different mechanisms which cause damage to a coating and can depend on both average and peak optical intensity [17]. For continuous wave lasers the damaging mechanism is based on thermal effects. Hereby, a thermal equilibrium arises between absorbed laser light and heat dissipated through the coating and the substrate. At a certain threshold the steady state temperature causes damage to the coating.

A comparison of two spot sizes of an incident laser shows the LIDT dependence on spot size and substrate material. When the spot size is small compared to the coating thickness, the heat produced by the absorbed laser light can dissipate along the coating and into the substrate. When the spot size is large compared to the coating thickness, the heat has to dissipate through the substrate. Thus, a higher thermal conductivity of the coating compared to the thermal conductivity of the substrate leads to a spot size dependence of the LIDT.

Figure 7 shows the LIDT set-up. First the laser beam is widened and collimated by a set of lenses. A 140 mm focus lens then focuses the beam onto the sample mirror. The sample mirror is located on a translation stage which enables scanning along the propagation axis of the beam. The reflected beam is redirected to a power meter to monitor any change of the reflected power indicating arising damage. A CCD camera was also used to observe stray light which would indicate a damaged spot on the coating. A spot with minimal stray light was chosen to avoid any influences of stray centers which indicate voids, defects or particles. These would decrease the LIDT [18,19].

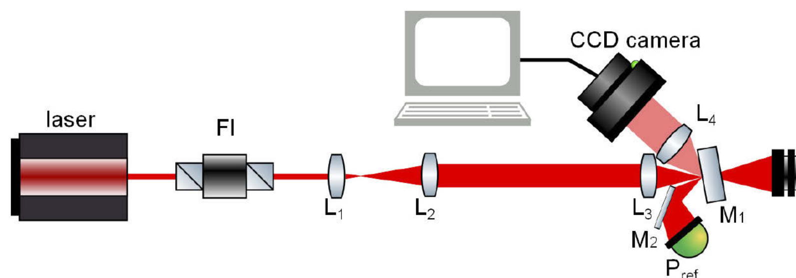

Fig. 7. A 1064 nm laser protected by a Faraday isolator (FI) is widened and collimated by a pair of lenses (L_1 with f = 50 mm and L_2 with f = 200 mm). The laser then is focused by L_3 (f = 140 mm) onto a GaAs/AlGaAs mirror (M_1). The reflected beam is steered by another mirror (M_2) to a power meter (P_{ref}). Further a CCD camera in combination with L_4 is used to observe the scattered light.

We measured a lower limit of the LIDT of a GaAs/AlGaAs coating to be 64 MW/cm^2 by focusing a 85 W continuous wave laser to a spot size of 9.2 μm radius. A 1064 nm wavelength laser was used for a highly reflective, substrate-transferred GaAs/AlGaAs coating with a center

Optics EXPRESS

wavelength of 1064 nm bonded to a fused silica substrate. A lens with a focal length of 140 mm was used to focus a 0.55 cm radius, collimated 85 W laser beam. This resulted in a corresponding power density of 64 MW/cm^2 or a linear power density of 46.2 kW/cm. A knife edge beam profiler was used to confirm the spot size and exclude lens errors such as spherical aberration. Neither reflected nor scattered light indicated any damage to the GaAs/AlGaAs coating. The measured LIDT value is well above the power density used in aLIGO at 17 kW/cm^2 [8].

8. Conclusion

We used a new method to measure the thickness uniformity of a GaAs/AlGaAs coating and showed that this comes very close to the needs of high precision interferometers. The measured thickness uniformity of 0.41 ± 0.05 nm RMS over a 4 cm diameter compares well with that of current IBS coatings.

Additionally we measured a lower limit of 64 MW/cm^2 for the continuous wave laser induced damage threshold for a substrate-transferred, highly reflective GaAs/AlGaAs coating.

Funding

Deutsche Forschungsgemeinschaft (EXC-2123/1); Max Planck Research School on Gravitational Wave Astronomy.

References

1. P. Aufmuth and K. Danzmann, "Gravitational wave detectors," New J. Phys. **7**, 202 (2005).
2. G. M. Harry, "Advanced LIGO: the next generation of gravitational wave detectors," Classical Quantum Gravity **27**(8), 084006 (2010).
3. G. D. Cole, W. Zhang, M. J. Martin, J. Ye, and M. Aspelmeyer, "Tenfold reduction of brownian noise in high-reflectivity optical coatings," Nat. Photonics **7**(8), 644–650 (2013).
4. G. D. Cole, W. Zhang, B. J. Bjork, D. Follman, P. Heu, C. Deutsch, L. Sonderhouse, J. Robinson, C. Franz, A. Alexandrovski, M. Notcutt, O. H. Heckl, J. Ye, and M. Aspelmeyer, "High-performance near- and mid-infrared crystalline coatings," Optica **3**(6), 647–656 (2016).
5. M. Marchiò, R. Flaminio, L. Pinard, D. Forest, C. Deutsch, P. Heu, D. Follman, and G. D. Cole, "Optical performance of large-area crystalline coatings," Opt. Express **26**(5), 6114–6125 (2018).
6. G. Billingsley, "Advanced ligo end test mass(etm)," https://dcc.ligo.org/LIGO-E080512/public (2009).
7. L. Pinard, C. Michel, B. Sassolas, L. Balzarini, J. Degallaix, V. Dolique, R. Flaminio, D. Forest, M. Granata, B. Lagrange, N. Straniero, J. Teillon, and G. Cagnoli, "Mirrors used in the LIGO interferometers for first detection of gravitational waves," Appl. Opt. **56**(4), C11–C15 (2017).
8. The LIGO Scientific Collaboration, "Advanced LIGO," Classical Quantum Gravity **32**(7), 074001 (2015).
9. S. J. Orfanidis, "multidiel," http://eceweb1.rutgers.edu/orfanidi/ewa/ (2016).
10. S. J. Orfanidis, "Electromagnetic waves and antennas," http://eceweb1.rutgers.edu/orfanidi/ewa/ewa-2up.pdf (2013).
11. H. A. MacLeod, *Thin-Film Optical Filters (Series in Optics and Optoelectronics)* (CRC Press, 2010).
12. J. Rheims, J. Köser, and T. Wriedt, "Refractive-index measurements in the near-IR using an abbe refractometer," Meas. Sci. Technol. **8**(6), 601–605 (1997).
13. I. H. Malitson, "Interspecimen comparison of the refractive index of fused silica," J. Opt. Soc. Am. **55**(10), 1205–1209 (1965).
14. U. P. V Holy and T Baumbach, *High-Resolution X-Ray Scattering from Thin Films and Multilayers* (Springer, 1999).
15. J. Li, S. M. Hill, J. A. Middlebrooks, C. Y. Chen, W. Li, J. M. Kuo, K. W. Vargason, Y. C. Kao, and P. R. Pinsukanja, "Highly uniform vcsels grown by multi-wafer production mbe," in *International Conference on Compound Semiconductor Manufacturing Technology (CS MANTEC)*, (2018).
16. G. W. DeBell, "Ion beam sputtered coatings for high fluence applications," in *Laser-Induced Damage in Optical Materials: 2005*, G. J. Exarhos, A. H. Guenther, K. L. Lewis, D. Ristau, M. Soileau, and C. J. Stolz, eds. (SPIE, 2005).
17. X. Wang, Z. H. Shen, J. Lu, and X. W. Ni, "Laser-induced damage threshold of silicon in millisecond, nanosecond, and picosecond regimes," J. Appl. Phys. **108**(3), 033103 (2010).
18. N. Bloembergen, "Role of cracks, pores, and absorbing inclusions on laser induced damage threshold at surfaces of transparent dielectrics," Appl. Opt. **12**(4), 661–664 (1973).
19. M. F. Koldunov and A. A. Manenkov, "Theory of laser-induced inclusion-initiated damage in optical materials," Opt. Eng. **51**(12), 121811 (2012).

194.95.157.39 {ts '2021-02-17 07:07:32'}